


Steady-state model for the three-leg shunt-series ac-link power flow controller

ISSN 1751-8687
 Received on 20th January 2015
 Revised on 14th July 2015
 Accepted on 2nd August 2015
 doi: 10.1049/iet-gtd.2015.0068
 www.ietdl.org

Manuel Barragán-Villarejo, Alejandro Marano-Marcolini, Jose Maria Maza-Ortega ,
 Antonio Gómez-Expósito

Department of Electrical Engineering, University of Sevilla, Avda. De los Descubrimientos s/n, 41092 Sevilla, Spain
 ✉ E-mail: jmmaza@us.es

Abstract: Shunt-series ac links constitute a class of so-called vector switching converters, capable of controlling power flows by synthesising an adjustable series voltage. A novel steady-state model for the recently introduced three-leg shunt-series ac link, suitable for power flow studies, is developed in this study. The new model is then applied in two optimal power flow problems arising in distribution systems, namely, power loss reduction and integration of distributed generation, where the performance of the three-leg topology is compared with that of the conventional four-leg scheme. The CIGRE Task Force C06.04.02 benchmark network is used as case study.

1 Introduction

Medium-voltage (MV) distribution networks are usually composed of a number of arborescent feeders linking the primary substation with a switching centre where normally open switches are located, as can be seen in Fig. 1a.

The switching centre reduces to just two adjacent feeders in the simplest case and is used to reduce the restoration time in case of failure of any of the interconnected feeders. This involves previously isolating the faulted zone followed by energisation of the healthy part by closing the respective mechanical switch. While this strategy has proved satisfactory for the distribution systems of the last century (i.e. passive networks with reduced measurement and automation resources) it is clearly insufficient in the upcoming smart grid context [1]. The new distribution business is facing the integration of new agents such as: distributed generators (DGs), electrical vehicles, massive installation of smart meters and much higher automation levels brought about by the introduction of ubiquitous information and communication technologies (ICTs) [2].

The transition to the new paradigm cannot be solely based on the application of new ICTs to the traditional business. As a matter of fact, one of the key objectives of the smart grid is to allow power flows to be controlled in a more flexible fashion [3, 4], which cannot be obviously achieved if the radial operation is maintained. To overcome this technical barrier, it has recently been proposed to 'loop' the radial feeders by means of power electronic devices substituting the normally open switches, as shown in Fig. 1b [5–7].

Earlier works introducing flexible links were based on power converters comprising an asynchronous dc link [8]. A comprehensive comparison of different dc-link topologies can be found in [7] where a novel operational scheme of the Unified Power Flow Controller (UPFC), termed UPFC-P0Q, is proposed capable of controlling only the active and reactive power flows across the interconnected feeders. Therefore, a degree of freedom is lost compared with the traditional back-to-back topology which can separately control the reactive power injections at both feeder terminals. The main advantage, however, of the UPFC-P0Q topology is that the rated power involved in power electronic devices is significantly reduced.

However the UPFC-P0Q is not the only topology providing two degrees of freedom. Some alternatives based on direct ac–ac topologies, such as vector switching converters (VeSCs), are also of interest owing to their inherent simplicity [9], the absence of

large dc capacitors and lower power rating of the semiconductor devices [10]. Some recent publications have appeared exploring the possibilities of power flow control using this new concept [9–11]. Those pioneering works analyse the converter topologies [12], develop both steady-state and dynamic models in order to assess their capability for power flow regulation, contribution to transient stability and voltage control [13–18], and present experimental validations through laboratory setups of a four-leg shunt-series controller [11] and a three-leg dynamic voltage restorer [19]. The most promising topology within this group is the so-called Γ controller (see Fig. 2a) which is a shunt-series arrangement capable of independently controlling the active and reactive powers exchanged between two networks [13].

A simpler alternative to the standard Γ topology has been recently proposed in [20] (see Fig. 2b), where a dynamic model is developed for this new topology and two strategies to control power flows are implemented and compared. In spite of being also a shunt-series arrangement, the following important differences can be pointed out between both topologies:

- The standard Γ controller is a three-phase four-leg device (12 two-quadrant type power electronic switches required), whereas the new device proposed in [20] comprises only three legs per phase (only nine two-quadrant type power electronic switches required). In the sequel, this arrangement will be termed the 3L- Γ controller.
- The shunt transformer used to supply the input voltages to the VeSC comprises five windings (Dd0y5d6y11 connection) in the Γ controller, whereas just a four-winding Yy0y0y0 transformer is required for the 3L- Γ topology.

Such differences preclude the use of the steady-state model of the Γ controller, built around an ideal transformer with variable transformation ratio depending on the duty cycles, for the 3L- Γ controller. Therefore, the main objective of this paper is to develop a steady-state model for the 3L- Γ converter suitable for power flow studies or secondary control applications which can rely just on phasors. Note that such applications usually run in the distribution management system represented in Fig. 1b, where the goal is to determine, usually with the help of an optimal power flow (OPF), the set points for the controllable resources along the distribution system to achieve an optimised operation. The proposed model takes into account active and reactive power losses (including those of power electronic devices and

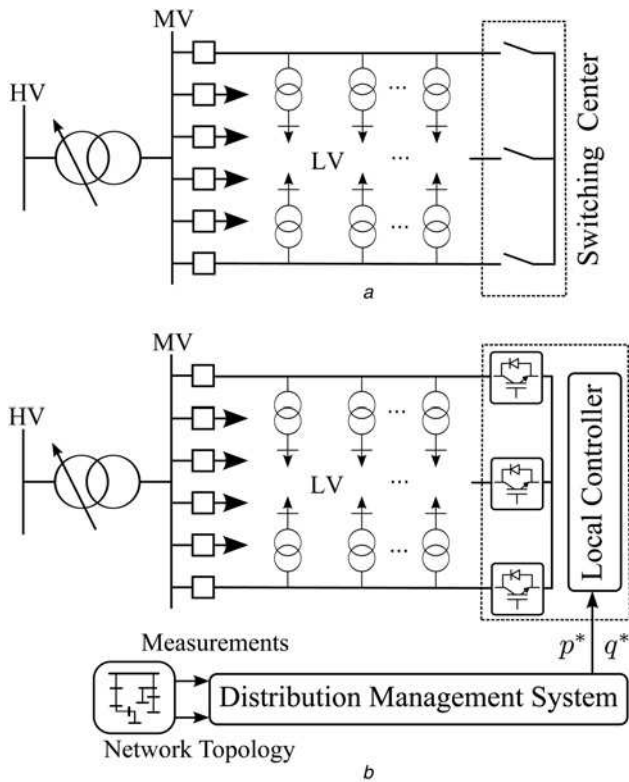


Fig. 1 MV distribution system

a Traditional scheme based on mechanical switches
b New scheme incorporating controllable links

transformers) which can be considered an additional contribution with respect to [17], where the Γ controller is represented by a lossless model.

This paper is organised as follows. Section 2 proposes a steady-state model for the 3L- Γ topology. On the basis of this model, Section 3 then establishes the operational restrictions of the 3L- Γ controller, which are compared with those of the standard Γ controller. Section 4 presents a case study based on the distribution network proposed by the CIGRE Task Force C06.04.02, intended to illustrate the differences between both topologies when ohmic losses are minimised or renewables penetration is maximised through an OPF algorithm.

2 Steady-state model of the 3L- Γ controller

This section is devoted to developing a full phasor model for the 3L- Γ controller shown in Fig. 2*b*, suitable for steady-state network applications, such as power flow or OPF algorithms.

The power flow controlling capability of this configuration stems from the voltage source inserted in the series branch. This voltage is synthesised as the weighted average of the input voltages, the weighting factors being related to the duty cycles of the converter [9].

The VeSC input voltages depend on the arrangement of the shunt multi-winding transformer, as follows

$$\mathbf{v}_{in1} = \mathbf{v}_{in2} = \mathbf{v}_{in3} \simeq \frac{1}{a_p} \mathbf{v}_1 \quad (1)$$

where a_p is the shunt transformer turns ratio and $\mathbf{v}_1 = [v_1^a, v_1^b, v_1^c]^T$ represents the abc phase voltages at feeder 1, assuming that the voltage drop across the transformer short-circuit reactance can be neglected. The duty ratios are determined by the control algorithm in order to obtain the reference power flow between the interconnected feeders. It is worth mentioning that those duty

ratios are of the dc-based type as explained in [9]. Considering the input voltages and the duty ratios, as illustrated in Fig. 2*b*, the output voltages, $\mathbf{v}_{out} = [v_{out}^a, v_{out}^b, v_{out}^c]^T$, and the input currents, \mathbf{i}_{inj} for $j = 1, 2, 3$, are defined as [20]

$$\mathbf{v}_{out} = \frac{1}{a_p} \begin{bmatrix} d_1 & d_2 & d_3 \\ d_3 & d_1 & d_2 \\ d_2 & d_3 & d_1 \end{bmatrix} \mathbf{v}_1 \quad (2)$$

$$\mathbf{i}_{in1} = [i_{in1}^a, i_{in1}^b, i_{in1}^c]^T = d_1 [i_{out}^a, i_{out}^b, i_{out}^c]^T$$

$$\mathbf{i}_{in2} = [i_{in2}^a, i_{in2}^b, i_{in2}^c]^T = d_2 [i_{out}^c, i_{out}^b, i_{out}^a]^T \quad (3)$$

$$\mathbf{i}_{in3} = [i_{in3}^a, i_{in3}^b, i_{in3}^c]^T = d_3 [i_{out}^b, i_{out}^c, i_{out}^a]^T$$

where $\mathbf{i}_{out} = [i_{out}^a, i_{out}^b, i_{out}^c]^T$ are the VeSC output currents. Note that the duty cycles must verify

$$\sum_{i=1}^3 d_i(t) = 1. \quad (4)$$

The currents flowing through the primary winding of the shunt input transformer, \mathbf{i}_{sh} , are related to the input currents of the VeSC as

$$\mathbf{i}_{sh} = \frac{1}{a_p} (\mathbf{i}_{in1} + \mathbf{i}_{in2} + \mathbf{i}_{in3}). \quad (5)$$

In the following, the analysis will be focused on phase a , in order to obtain the single-phase equivalent defining the phasor model for the 3L- Γ controller. According to (1) and (2), the output voltage v_{out}^a is

$$v_{out}^a = \frac{1}{a_p} (d_1 v_1^a + d_2 v_1^b + d_3 v_1^c) \quad (6)$$

and the relationship between primary and secondary currents in the shunt transformer is obtained from

$$i_{sh}^a = \frac{1}{a_p} (i_{in1}^a + i_{in2}^a + i_{in3}^a) \quad (7)$$

Finally, the shunt current is computed taking into account (3), and relating the VeSC output current, \mathbf{i}_{out} , with the line current, \mathbf{i}_2 , through the series transformer turns ratio a_s

$$i_{sh}^a = \frac{1}{a_p} (d_1 i_{out}^a + d_2 i_{out}^c + d_3 i_{out}^b) = -\frac{a_s}{a_p} (d_1 i_2^a + d_2 i_2^c + d_3 i_2^b) \quad (8)$$

Equations (6) and (8) show a similar structure, however, the duty ratios d_2 and d_3 are multiplying the phase voltages b and c in (6) and the phase currents c and b in (8). This fact has important implications for the developed phasor model, as explained in the sequel. Note that the Γ controller is modelled as an ideal transformer, in which the turns ratio is equal to the duty cycle [17], because each duty cycle multiplies the same phase magnitudes for both series voltage and shunt current equations. However, that is not the case of the 3L- Γ controller, as clearly seen from (6) and (8). Therefore, the 3L- Γ controller cannot be directly represented by a transformer with the turns ratio depending on the duty cycles. As a consequence, the single-phase equivalent circuit proposed for the 3L- Γ controller is based on two dependent sources, as depicted in Fig. 3: a series voltage source and a shunt current source according to (6) and (8), respectively. The model is completed by including the short-circuit reactances of the shunt and series transformers, X_{sh} and X_s , respectively.

Even though the magnitudes of the dependent current and voltage sources shown in Fig. 3 are formulated as a function of the duty

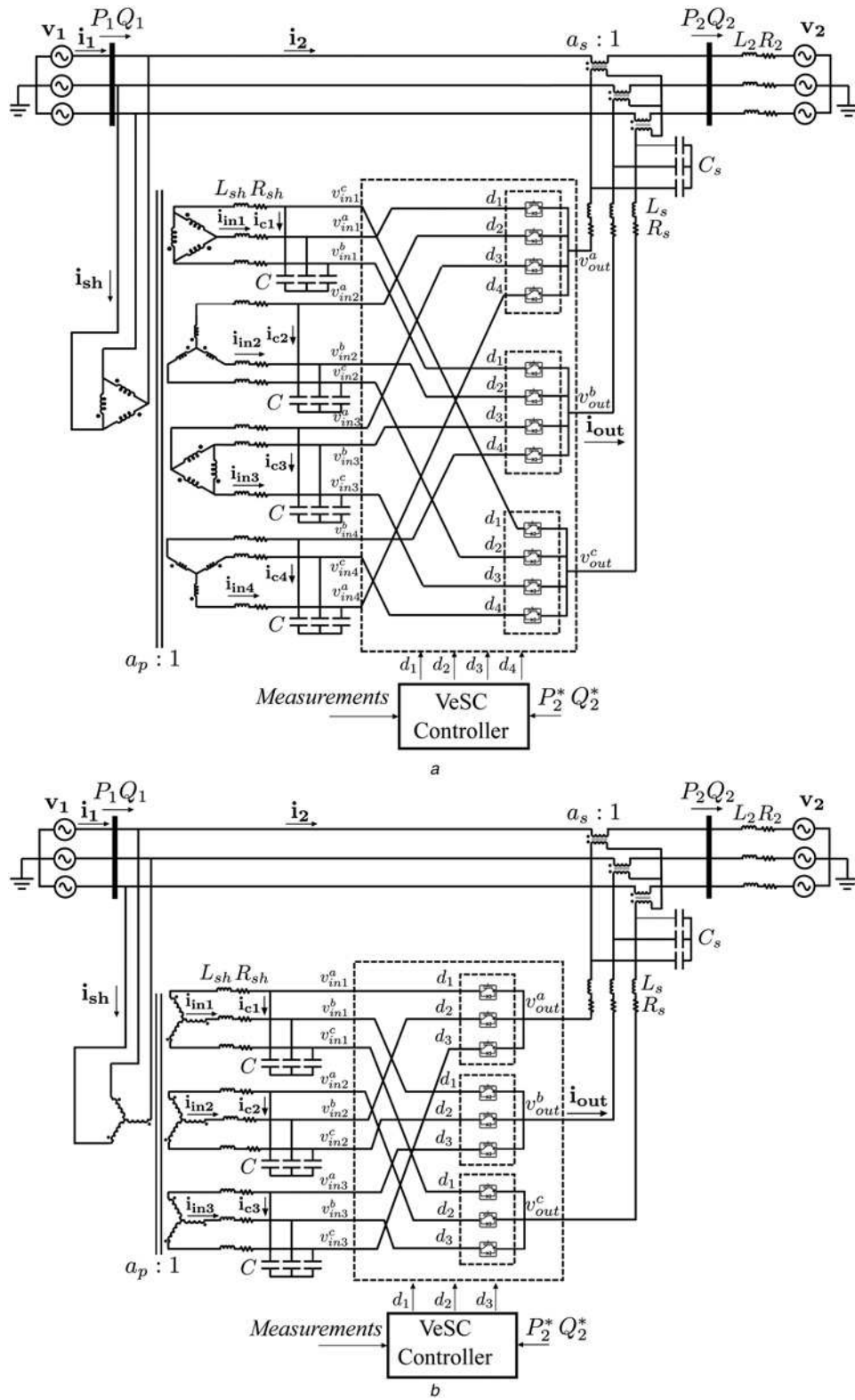


Fig. 2 Γ controller
 a Conventional Γ shunt-series controller
 b 3L- Γ shunt-series controller

ratios, it is interesting to introduce a new set of variables to simplify the control algorithm. Since the objective of the 3L- Γ device is to control the active and reactive power flows between the interconnected feeders by means of the series voltage V_s , it makes sense to decompose it into two orthogonal components, as shown in Fig. 4. This allows a straightforward formulation of the active and reactive power flows [20]

$$V_s \simeq a_s V_{out} = V_{sQ} + jV_{sP} = (d_Q + jd_P) \frac{a_s}{a_p} V_1 \quad (9)$$

where the voltage drop related to the short-circuit reactances of the shunt and series transformers has been neglected. As a consequence, a new definition of the duty ratios d_P and d_Q , which extraordinarily simplifies the control algorithm, is proposed. Note

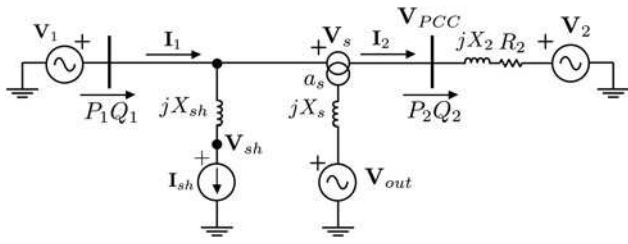


Fig. 3 Single-phase 3L-Γ equivalent circuit for phase a

that these duty ratios are related to the original ones by

$$\begin{bmatrix} d_Q \\ d_p \end{bmatrix} = \begin{bmatrix} 1 & -0.5 & -0.5 \\ 0 & -\sqrt{3}/2 & \sqrt{3}/2 \end{bmatrix} \begin{bmatrix} d_1 \\ d_2 \\ d_3 \end{bmatrix} \quad (10)$$

The operational constraints of the newly defined duty cycles considering (4) and (10) can be stated as

$$d_Q \in [-0.5, 1], \quad d_p \in \left[\frac{d_Q - 1}{\sqrt{3}}, \frac{1 - d_Q}{\sqrt{3}} \right] \quad (11)$$

Similarly, the shunt current of the equivalent circuit shown in Fig. 3, I_{sh} , can be formulated as a function of the new duty ratios as follows. First, the time-domain formulation of the current in (8) is transformed to the phasor domain, considering that the currents are balanced

$$I_{sh} = -\frac{a_s}{a_p} I_2 (d_1 + d_2 e^{j2\pi/3} + d_3 e^{-j2\pi/3}) \quad (12)$$

Second, the relationship between the proposed duty cycles d_Q and d_p and the original ones d_1, d_2 and d_3 , given by (4) and (10), are introduced in the previous equation, yielding

$$I_{sh} = -\frac{a_s}{a_p} I_2 (d_Q - j d_p) \quad (13)$$

Finally, the current I_2 is computed using the following voltage equations, easily derived from Fig. 3

$$V_1 = V_s + I_2(R_2 + jX_2) + V_2 \quad (14)$$

$$a_s V_{out} = V_s - I_2 a_s^2 (R_s + jX_s) \quad (15)$$

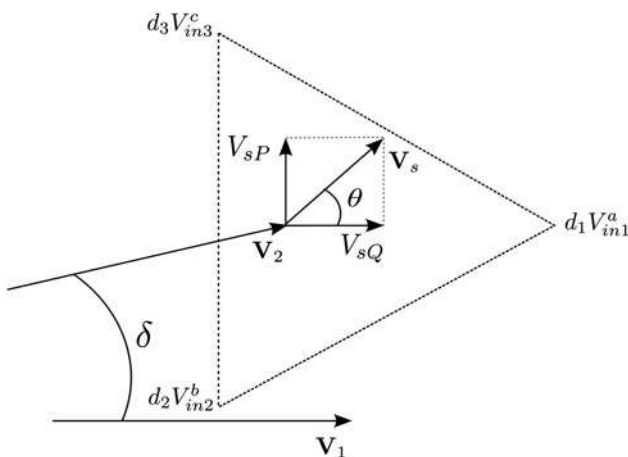


Fig. 4 Voltage phasor diagram and orthogonal decomposition of V_s

yielding

$$I_2 = \frac{V_1 - a_s^2/a_p (d_Q + j d_p) V_1 - V_2}{(R_2 + a_s^2 R_s) + j(X_2 + a_s^2 X_s)} \quad (16)$$

Therefore, the shunt current I_{sh} and the series voltage V_{out} are defined as a function of the duty cycles, d_p and d_Q , the transformer reactances, X_{sh} and X_s , and the voltages of the systems V_1 and V_2 .

The model is completed by adding the active and reactive power flow balances for the whole system

$$P_1 - P_2 - P_{loss}^{VeSC} = 0 \quad (17)$$

$$Q_1 - Q_2 - Q_s - Q_{sh} = 0 \quad (18)$$

where P_1, P_2, Q_1 and Q_2 are the active and reactive power flows through each feeder, Q_s and Q_{sh} are the reactive power losses related to the series and shunt transformers and P_{loss}^{VeSC} corresponds to the active power losses of the VeSC. A comprehensive analysis of these losses can be found in [10].

3 Comparison of the feasible operating regions

In this section, the feasible operating regions of the Γ and 3L- Γ controllers will be compared in terms of active and reactive power flows between the interconnected feeders, assuming similar ratings for both devices.

The feasible operating regions of the Γ and 3L- Γ controllers are shown in Fig. 5 for a distribution power system characterised by the parameters detailed in Table 1. This figure shows the active and reactive powers that can be exchanged between the interconnected power systems using these devices with the same rated voltages and currents. Both operating areas are derived from the maximum series voltage introduced between the radial feeders. Keeping this in mind, the operational area of the Γ controller lies inside the circumference inscribed in the square formed by the output voltages of the four-poles VeSC used in this topology, as defined in [13]. Correspondingly, the allowed operating area of the 3L- Γ controller is derived from the triangle resulting of the output voltages of the three-poles VeSC. It can be noted in Fig. 5 that, in

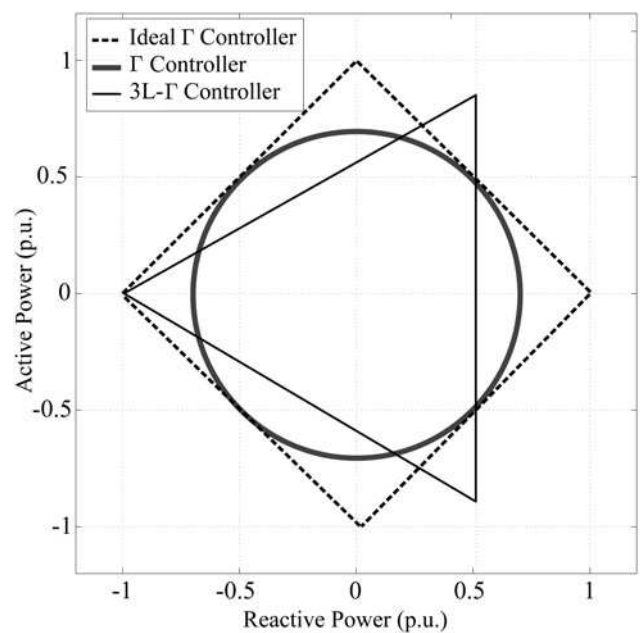


Fig. 5 Feasible operating region of the Γ and 3L- Γ controllers for the data shown in Table 1

terms of surface size, the operating region corresponding to the Γ controller is larger, in accordance with the higher number of windings in the shunt transformer.

A comprehensive comparison, however, cannot be based solely on the total surface of the operational region, being it necessary to include a more thorough quantitative analysis with the help of the performance indices proposed in [7]. Those indices compare both the size and shape of the operating region for each of the analysed topologies, which is crucial to determine their capability to keep separately under control the active and reactive power flows. For this purpose, the feasible region (FR) is discretised into a grid of small enough squares. Each square i is characterised by three parameters: x_i , P_i and Q_i . The first one, x_i , indicates if the small discretised square is within ($x_i=1$) or without ($x_i=0$) the FR of the analysed controller. The latter ones refer to the active and reactive power flows between the feeders related to the square i . According to these parameters the following performance indices can be defined:

- **FR ratio:** This index reflects the size of the FR

$$R_{FR} = \sum_i x_i \rightarrow x_i = \begin{cases} 0, & i \notin FR \\ 1, & i \in FR \end{cases} \quad (19)$$

- **Active power ratio:** This index reflects the ability of the power electronic-based device to control the active power flow between the feeders

$$R_p = \sum_{i \in FR} P_i \quad (20)$$

- **Reactive power ratio:** This ratio measures the ability of the power electronic-based device to control the reactive power injected into the feeders

$$R_Q = \sum_{i \in FR} Q_i \quad (21)$$

Table 1 Parameters of the benchmark system used in the comparison of the operating region of the ac-based link devices

Parameters	Value
rated voltage, V_1 and V_2	20 kV
base power, S_{base}	10 MVA
angles, θ_1 and θ_2	0°
line impedance, $R_2 + jX_2$	$0.003 + j0.003$ pu
maximum current, I_{max}	1 pu
converter	
rated power, S_{rat}	250 kVA
series reactance, X_s	0.0025 pu
shunt reactance, X_{sh}	4 pu
series-rated current, I_s^{rat}	1.05 pu
series-rated voltage, U_s^{rat}	0.12 pu

The following relative indices are computed for the 3L- Γ topology when those of the Γ controller are taken as reference

$$\frac{R_{FR}^{3L-\Gamma}}{R_{FR}^\Gamma} = 0.82, \quad \frac{R_p^{3L-\Gamma}}{R_p^\Gamma} = 1.22, \quad \frac{R_Q^{3L-\Gamma}}{R_Q^\Gamma} = 1.05$$

In spite of the FR being larger for the Γ controller, the active and reactive power ratios corresponding to the simpler 3L- Γ device are better, which implies higher capability for controlling the active and reactive powers between the interconnected feeders. This shows the suitability of the proposed 3L- Γ controller for flexible interconnection of adjacent distribution feeders.

4 Case studies

The steady-state model of the 3L- Γ device developed in Section 2 will be tested and validated in two different OPF scenarios typically arising in planning and operation of distribution feeders. In the first OPF problem, the objective function is to maximise the amount of distributed generation that can be tolerated by the feeder system. In the operation scenario, the objective is to reduce

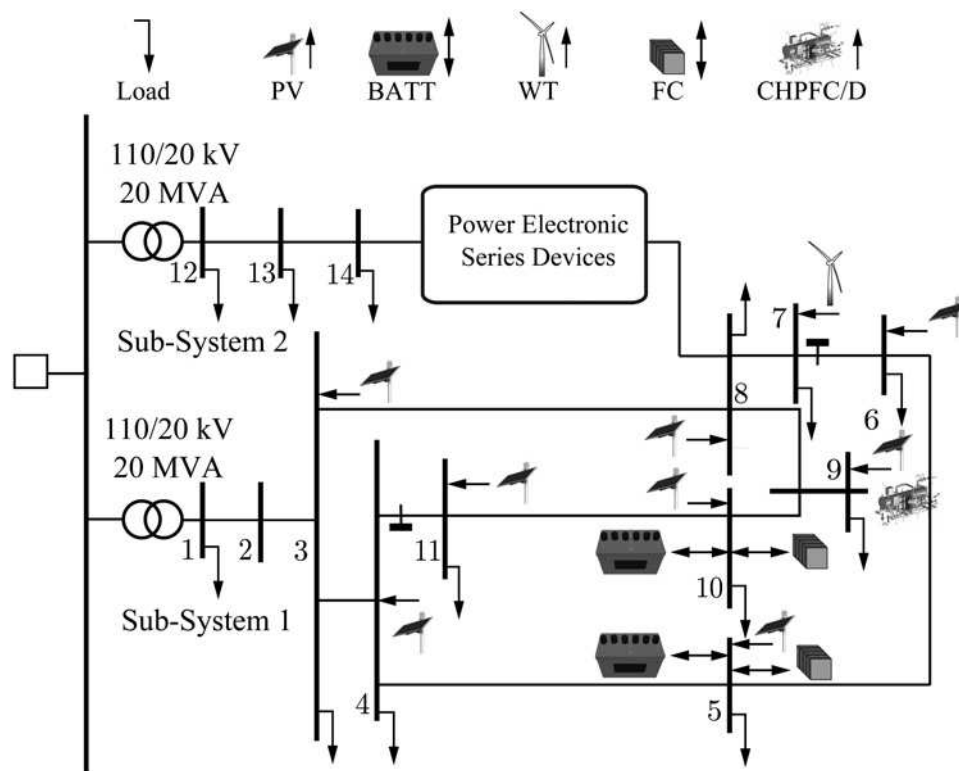


Fig. 6 Benchmark distribution system

Table 2 Technical data of the ac links (base power 10 MVA)

Topology	S_{rat} , MVA	a_{sr} , pu	a_{pr} , pu	X_{sr} , pu	X_{shr} , pu
Γ	0.6	1	16	0.00625	1.6
3L- Γ	0.6	1	16	0.00625	1.6

Table 3 Results of the planning scenario

	Δ DG, MW	Constraint (capacity)
base case	18.38	lines 2-3, 7-8 and 8-3
Γ controller	27.5	lines 2-3, 8-9 and 8-3, ac link
3L- Γ controller	27.6	lines 2-3 and 7-8, ac link

the active power losses of the system. In both scenarios, the two degrees of freedom of the shunt-series power converters will be considered as additional control variables aimed at equalising the feeder loading levels. As a byproduct, the performance of the Γ and 3L- Γ controllers will be compared. The model adopted to describe the Γ controller can be found in [17].

The benchmark distribution system used for both case studies is shown in Fig. 6. It is composed of two subsystems fed from the same distribution substation. The subsystem 1 has several DGs with different types of primary energy sources and storage systems with different daily profiles. It is worth mentioning that the batteries have not been considered as active control variables in this paper. On the other hand, no DGs are connected to subsystem 2. The consumers are classified either as industrial or residential loads, each with its own daily profiles. An extra load (3 MW and 1 Mvar) is added to bus 6 in subsystem 1, so that this subsystem is considerably more loaded than subsystem 2 and the benefits of adding ac links between both feeders become more apparent. All the data related to this benchmark distribution system including the line parameters and daily profiles of loads, generators and storage systems can be found in [21].

The ac link (Γ or 3L- Γ controller) is placed between buses 8 and 14, corresponding to subsystems 1 and 2, respectively. In the planning

scenario, the ac link will transfer active and reactive powers from the congested subsystem (limited by either ampacity or voltage violation) to the less loaded one, allowing a larger injection of active power from DGs. In the operation scenario, the ac link will try to transfer active power from the least loaded subsystem, reducing in this way the active power losses of the whole system.

The main technical data corresponding to each ac link are provided in Table 2. The apparent power that the ac link can shift between the interconnected buses (8 and 14) is limited to 9 MVA, in accordance with the most restrictive ampacity of upstream branches. Note, however, that such a high power can be managed by converters of much smaller rated power ($S_{rat} = 0.6$ MVA). The Γ controller has 12 solid-state switching devices [insulated gate bipolar transistors (IGBTs)], whereas the 3L- Γ topology has only 9. This highly influences the internal power losses of the devices, which is one of the advantages of the subject topology of this paper.

4.1 Performance of the ac links in the planning scenario

The performance of the power electronic-based devices is assessed in terms of their capability to increase the active power that can be injected by the DGs. The selected scenario corresponds to the hour of the day with the highest solar radiation. The problem is formulated as an OPF in order to maximise the generation of DG keeping all operational constraints (bus voltages, line ampacities and converter ratings) in the FR. A brief overview of the OPF algorithm, including the control variables and the main equations, has been included in Appendix, but further details can be found in [22]. The optimisation problem is solved under the GAMS environment [23] with the non-linear CONOPT solver [24].

In the base case (i.e. without the ac link), the maximum distributed power which can be integrated into the network is 18.38 MW. This is limited by the saturation of lines connecting buses 2-3, 7-8 and 8-3. The additional generation comes from the photovoltaic generator at bus 3, the wind farm at bus 7 and the cogeneration groups of bus 9.

When the ac link is in operation, connecting both subsystems, the amount of power which can be integrated improves owing to the possibility of transferring active power from subsystem 1 (where all the DGs are located) to subsystem 2. It is worth mentioning

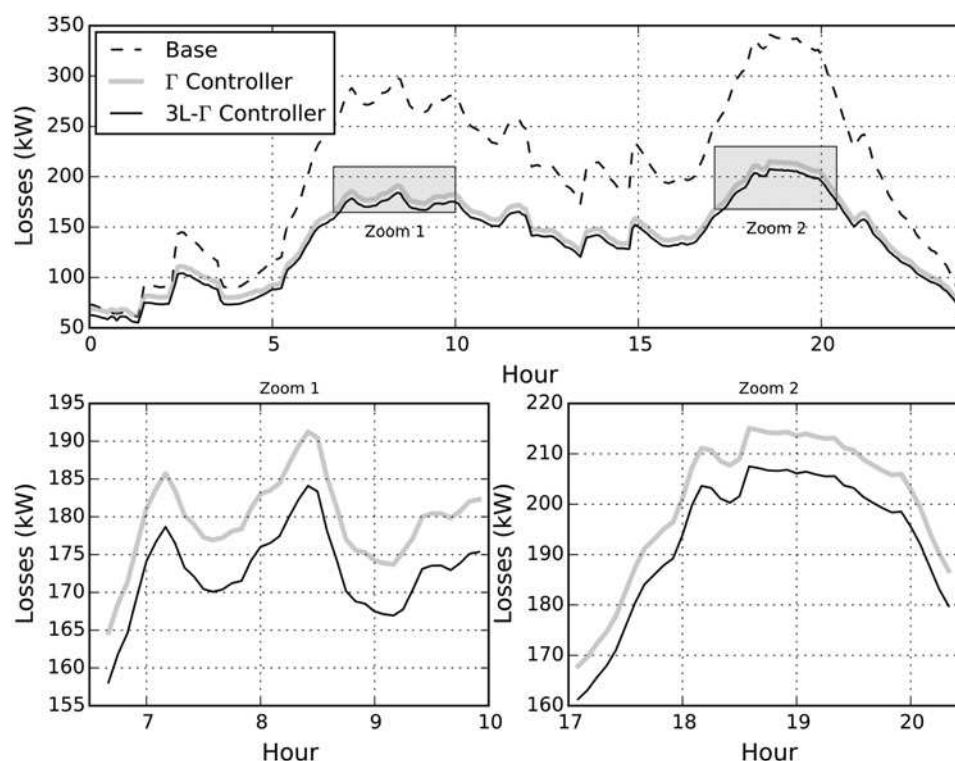
**Fig. 7** 24 h evolution of the total power losses. The lower graphics show the zoomed view during peak load periods

Table 4 24 h total energy losses in the benchmark distribution system

	Energy losses, kWh		Reduction, %
	VeSC	System	
base case	–	4904	–
Γ controller	89	3396	30.74
3L- Γ controller	70	3331	32.1

that both the Γ and the 3L- Γ controllers have a similar performance in this case. The results, collected in Table 3, show that the power injected by the DGs exceeds 27 MW in this situation. This is constrained by the ampacity of the distribution feeders and the capacity of the ac link.

4.2 Performance of the ac links in the operation scenario

A full day simulation is carried out to assess the additional benefits that can be gained from the incorporation of ac links in terms of power loss reduction. The simulation consists of a sequence of OPFs, performed at intervals of 5 min. A detailed description of the OPF can be found in [22, 25]. As in the planning case, the OPF is solved under the GAMS environment with the non-linear solver CONOPT.

In Fig. 7, the 24 h evolution of the active power losses is shown for different cases, with and without connecting devices. The energy losses of the system and the VeSC controllers for the whole day are given in Table 4. Both ac-link topologies achieve a significant reduction of active power losses. In addition, the power losses of the 3L- Γ device are lower than those of the conventional

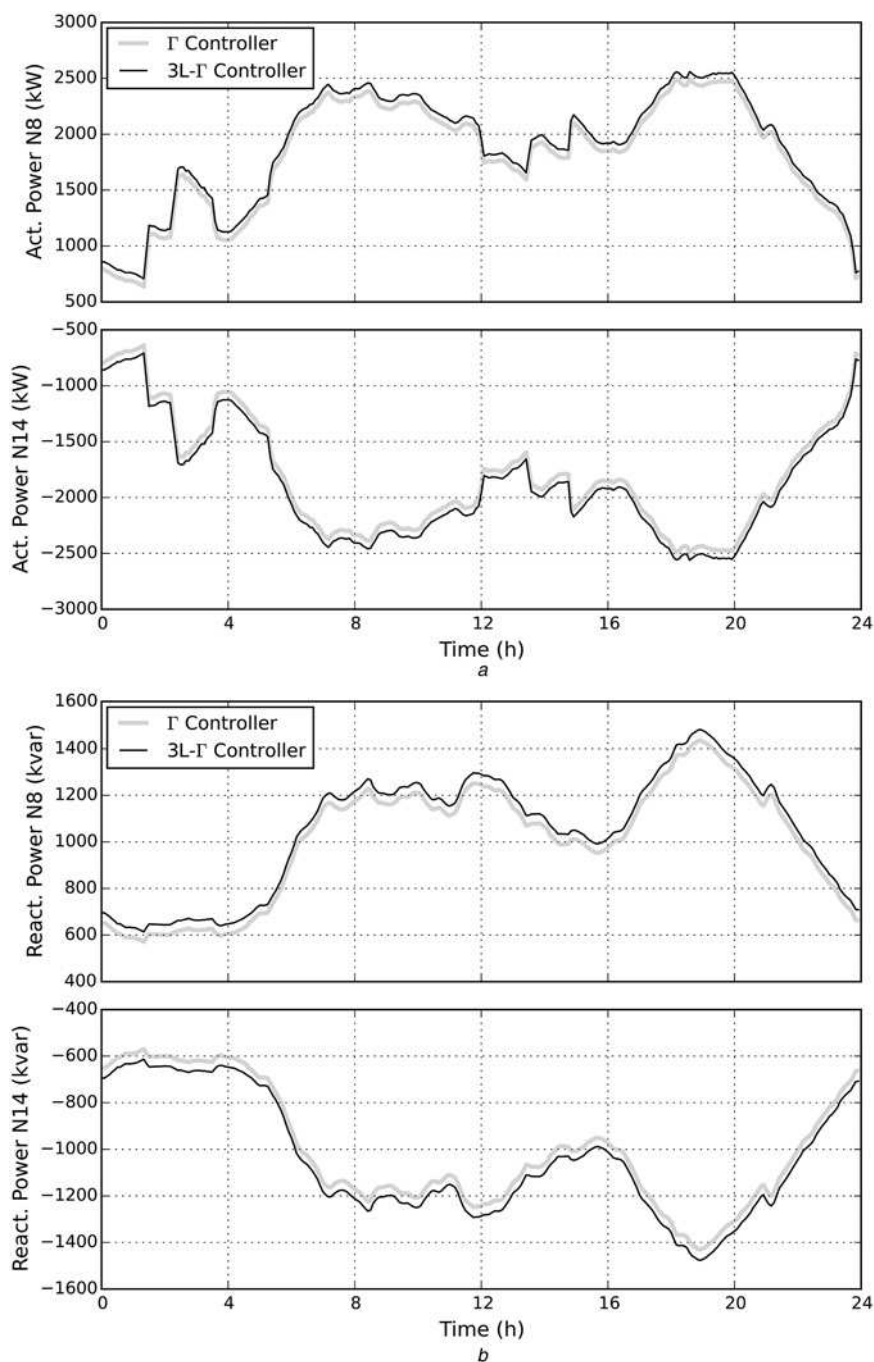


Fig. 8 Evolution of the

- a Active
- b Reactive powers injected into buses 8 and 14 by the ac links

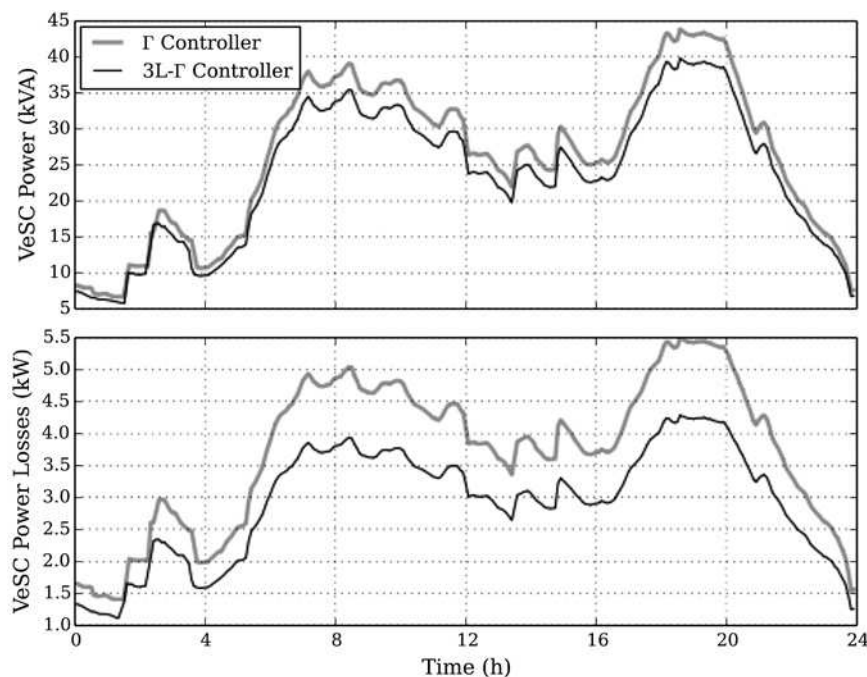


Fig. 9 Evolution of the apparent powers of the Γ and $3L\text{-}\Gamma$ and their active power losses

Γ controller, as a result of the reduced number of IGBTs. This helps total power losses to be reduced, as shown in Fig. 7.

Such a reduction in power losses stems from the flow of active and reactive powers between the 'bridged' feeders. Fig. 8 represents the daily evolution of the active and reactive powers injected (negative means absorbed) by the VeSC controllers into the terminal nodes. This figure reveals that, indeed, the ac links considered in this paper need to withdraw from bus 14 the active and reactive powers injected into bus 8 (plus the corresponding losses), as they have only two degrees of freedom. In other words, part of the subsystem 1 loads are fed from the subsystem 2, giving rise in the general multi-feeder case to a load equalisation throughout the system. Another important feature of the ac links studied in this work arises when analysing the apparent power of the power electronic devices,

which is shown in Fig. 9 along with the respective active power losses. Note that the apparent power is only a fraction of the power flows actually shifted between the radial feeders (see Fig. 8). Therefore, both ac links are advantageous in terms of reduced investment cost when compared with traditional dc back-to-back topologies. Moreover, as previously seen in Fig. 7, Fig. 9 clearly shows that the active power losses of the simpler $3L\text{-}\Gamma$ topology, comprising only nine solid-state switches, are lower than those of the original Γ controller (12 switches).

Finally, it is worth noting that both devices inject reactive power into bus 8, as shown in Fig. 8, in order to increase its voltage. As a matter of fact, the voltage at bus 8 (bus 14) increases (decreases) with respect to the base case, as shown in Fig. 10. This is a consequence of both active and reactive power being injected into bus 8 and withdrawn from bus 14.

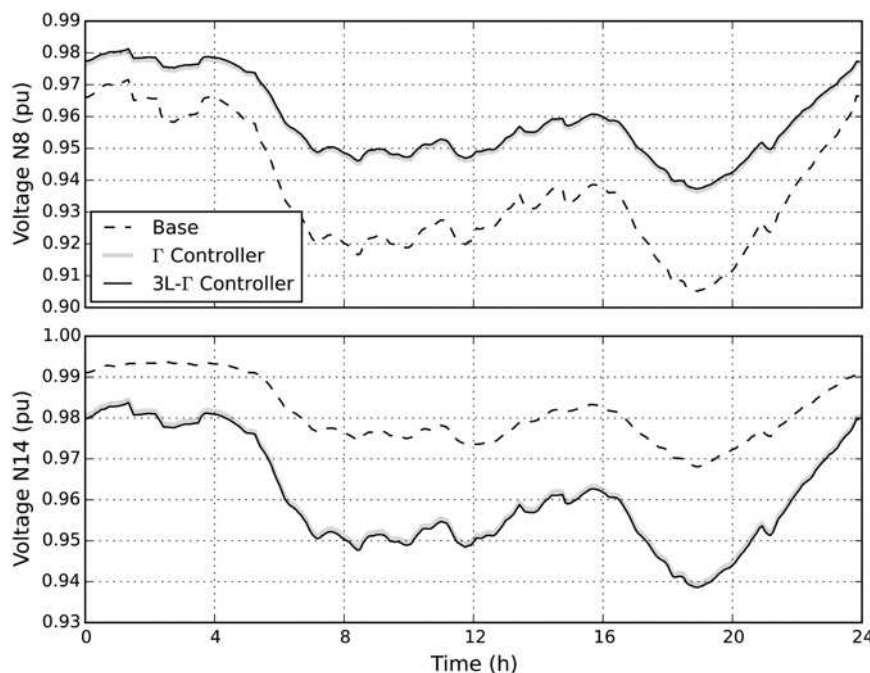


Fig. 10 Voltage evolution at buses 8 and 14

5 Acknowledgment

This work has been financially supported by the Andalusian Government and the Spanish Ministry of Economy and Competitiveness under grants TEP-07411 and ENE2011-24137, respectively.

6 Conclusions

A steady-state full model of the recently introduced 3L- Γ controller has been presented in this paper. The model, intended for power flow and OPF solutions, considers the reactive power losses associated to the series and shunt transformers as well as the active power losses of the power electronic switches. In developing such a model, the main difficulty stems from the fact that, unlike the standard Γ controller, the 3L- Γ topology cannot be modelled by means of an ideal transformer. Then, the newly developed model has been tested, and compared with that of the Γ controller, in the OPF solution of the CIGRE Task Force C06.04.02 benchmark distribution system. While both ac links are capable of significantly improving the operation of the feeder system, in terms of increased distributed generation penetration and power loss reduction, the 3L- Γ device has been identified as a better choice owing mainly to the reduced number of electronic switches (9 versus the 12 required by the Γ controller) and smaller power losses. This is achieved without sacrificing its capability for regulating active and reactive powers, as proved quantitatively by several performance indices also analysed in this paper.

6 References

- Lightner, E., Widergren, S.: 'An orderly transition to a transformed electricity system', *IEEE Trans. Smart Grid*, 2010, **1**, pp. 3–10
- Mallet, P., Granstrom, P.-O., Hallberg, P., *et al.*: 'Power to the people: European perspectives on the future of electric distribution', *IEEE Power Energy Mag.*, 2014, **12**, pp. 51–64
- European Commission: 'European technology platform smartgrids vision and strategy for Europe's electricity networks of the future' (European Smart Grids Technology Platform, 2006)
- HomChaudhuri, B., Kumar, M., Devabhaktuni, V.: 'Market based approach for solving optimal power flow problem in smart grid'. American Control Conf. (ACC), 2012, 2012, pp. 3095–3100
- Barragan, M., Mauricio, J., Marano, A., *et al.*: 'Operational benefits of multiterminal dc-links in active distribution networks'. 2012 IEEE Power and Energy Society General Meeting, 2012, pp. 1–6
- Marano-Marcolini, A., Romero-Ramos, E., Gomez-Exposito, A., *et al.*: 'Enhancing the integration of renewable sources in distribution systems using dc-links'. 2009 IEEE PES/IAS Conference on Sustainable Alternative Energy (SAE), 2009, pp. 1–5
- Maza-Ortega, J., Gomez-Exposito, A., Barragan-Villarejo, M., *et al.*: 'Voltage source converter-based topologies to further integrate renewable energy sources in distribution systems', *IET Renew. Power Gener.*, 2012, **6**, pp. 435–445
- Majumder, R.: 'Aspect of voltage stability and reactive power support in active distribution', *IET Gener. Transm. Distrib.*, 2014, **8**, pp. 442–450
- Venkataramanan, G.: 'Three-phase vector switching converters for power flow control', *IEE Proc., Electr. Power Appl.*, 2004, **151**, pp. 321–333
- Mancilla-David, F., Bhattacharya, S., Venkataramanan, G.: 'A comparative evaluation of series power-flow controllers using dc- and ac-link converters', *IEEE Trans. Power Deliv.*, 2008, **23**, pp. 985–996
- Mancilla-David, F., Venkataramanan, G.: 'Realisation of an ac link unified power flow controller', *IET Gener. Transm. Distrib.*, 2012, **6**, pp. 294–302
- Mancilla-David, F.: 'AC link vector switching converters for power flow control and power quality: a review'. North American Power Symp. (NAPS), 2009, pp. 1–7
- Mancilla-David, F., Venkataramanan, G.: 'A pulse width modulated ac link unified power flow controller', IEEE Power Engineering Society General Meeting, 2005, 2005, vol. 2, pp. 1314–1321
- Ramirez, J., Gonzalez, J.: 'Steady-state analysis of a novel UPFC'. IEEE Power Engineering Society General Meeting, 2006, 2006, p. 6
- Ramirez, J., Gonzalez, J.: 'Incorporating ac/ac controllers into a power flow formulation'. IEEE/PES Transmission Distribution Conf. and Exposition: Latin America, 2006. TDC '06, 2006, pp. 1–5
- Gonzalez, J., Ramirez, J.: 'AC-AC controller for steady state and transient stability analysis'. Power Symp., 2006, NAPS 2006, 38th North American, 2006, pp. 613–618
- Ramirez, J., Gonzales, J., Crow, M.: 'Steady state formulation of FACTS devices based on ac/ac converters', *IET Gener. Transm. Distrib.*, 2007, **1**, pp. 619–631
- Garcia-Vite, P.M., Mancilla-David, F., Ramirez, J.M.: 'Dynamic modelling and control of an ac-link dynamic voltage restorer'. IEEE Int. Symp. on Industrial Electronics (ISIE), 2011, pp. 1615–1620

- Garcia-Vite, P., Mancilla-David, F., Ramirez, J.: 'Per-sequence vector-switching matrix converter modules for voltage regulation', *IEEE Trans. Ind. Electron.*, 2013, **60**, pp. 5411–5421
- Barragan-Villarejo, M., Venkataramanan, G., Mancilla-David, F., *et al.*: 'Dynamic modelling and control of a shunt-series power flow controller based on ac-link', *IET Gener. Transm. Distrib.*, 2012, **6**, pp. 792–802
- Rudion, K., Orths, A., Styczynski, Z., *et al.*: 'Design of benchmark of medium voltage distribution network for investigation of DG integration'. IEEE Power Engineering Society General Meeting, 2006, 2006, p. 6
- Romero-Ramos, E., Gomez-Exposito, A., Marano-Marcolini, A., *et al.*: 'Assessing the loadability of active distribution networks in the presence of dc controllable links', *IET Gener. Transm. Distrib.*, 2011, **5**, pp. 1105–1113
- McCarl, B.: 'GAMS User Guide'. Version 23.6 2011. Available on-line at <http://www.gams.com>
- Drud, A.S.: 'CONOPT – a large scale GRG code', *ORSA J. Comput.*, 1994, **6**, pp. 207–216
- Acha, E., Fuerte-Esquivel, C.R., Ambriz-Pérez, H., *et al.*: 'FACTS: modelling and simulation in power networks' (Wiley, Chichester, UK, 2004)

7 Appendix: OPF description

This appendix describes the OPF used to model the steady-state behaviour of the 3L- Γ controller in the distribution network. A general formulation of an OPF can be stated as follows

$$\min f(\mathbf{x}, \mathbf{u}) \quad (22)$$

$$\text{s.t. } g(\mathbf{x}, \mathbf{u}) = 0 \quad (23)$$

$$h(\mathbf{x}, \mathbf{u}) \leq 0 \quad (24)$$

where $f(\mathbf{x}, \mathbf{u})$ is the objective function to be minimised subject to the equality and inequality constraints represented by $g(\mathbf{x}, \mathbf{u})$ and $h(\mathbf{x}, \mathbf{u})$, respectively, \mathbf{x} is the vector of state variables composed of the voltage magnitudes V_i and angles θ_i for every bus i and \mathbf{u} is the vector of control variables. This general formulation is valid to assess both, the planning and the operation scenarios, by just changing the set of active control variables and the objective function, as shown below.

The equality constraints are the active and reactive power balances for each bus

$$P_i^{\text{bal}} = V_i \sum_j (V_j G_{ij} \cos \theta_{ij} + V_j B_{ij} \sin \theta_{ij}) \quad (25)$$

$$Q_i^{\text{bal}} = V_i \sum_j (V_j G_{ij} \sin \theta_{ij} - V_j B_{ij} \cos \theta_{ij}) \quad (26)$$

$$P_i^{\text{bal}} = P_i^g - P_i^l, \quad \forall i - \{m, n\} \quad (27)$$

$$Q_i^{\text{bal}} = Q_i^g - Q_i^l, \quad \forall i - \{m, n\} \quad (28)$$

$$P_m^{\text{bal}} = P_m^g - P_m^l - P_1 \quad (29)$$

$$P_n^{\text{bal}} = P_n^g - P_n^l + P_2 \quad (30)$$

$$Q_m^{\text{bal}} = Q_m^g - Q_m^l - Q_1 \quad (31)$$

$$Q_n^{\text{bal}} = Q_n^g - Q_n^l + Q_2 \quad (32)$$

$$0 = P_1 - P_2 - P_{\text{loss}}^{\text{VeSC}} \quad (33)$$

$$0 = Q_1 - Q_2 - Q_s - Q_{\text{sh}} \quad (34)$$

where $P_i^g + jQ_i^g$ is the total complex power injected by dispersed generators connected to bus i , $P_i^l + jQ_i^l$ is the total complex load demanded at bus i , $G_{ij} + jB_{ij}$ is the ij -element of the bus admittance matrix; m and n are the ac-link connection buses. P_1 , P_2 and Q_1 , Q_2 are the active and reactive power injections to each

feeder by the ac link, respectively (the signs of these quantities are shown in Fig. 3). Finally, (33) and (34) indicate the active and reactive power balance through the ac link, where $P_{\text{loss}}^{\text{VeSC}}$ is the active power losses of the VeSC, and Q_s , Q_{sh} are the reactive power losses related to the series and shunt transformers, respectively.

Inequality constraints are defined as follows

$$0 \leq I_{ij} \leq I_{ij}^{\text{max}} \quad (35)$$

$$V_i^{\text{min}} \leq V_i \leq V_i^{\text{max}} \quad (36)$$

$$0 \leq S_{3L-\Gamma} \leq S_{\text{rat}} \quad (37)$$

Equation (35) is the conductor ampacity limit, (36) defines the bus voltage magnitude limits and (37) refers to the converter rated power limit.

The objective function and the control variables can be formulated as follows depending on the scenario:

- *Planning scenario*: The objective in this case is to maximise the penetration of DGs. Thus, the control variables \mathbf{u} are P_i^g for every DG and the ac-link active and reactive power injections, (P_2, Q_2) , whereas the objective function is

$$f_p(\mathbf{u}) = - \sum_{i=1}^{i=n} P_i^g \quad (38)$$

- *Operation scenario*. In this case the aim is to reduce the system losses as much as possible. The only decision variables in \mathbf{u} are the ac-link active and reactive power injections, (P_2, Q_2) , while the objective function is

$$f_o(\mathbf{x}) = P_{\text{loss}}(\mathbf{x}) \quad (39)$$